Canadian Science Publishing | Canadian Geotechnical Journal

Study on the horizontal bearing characteristics of pile foundation in coral sand

Journal:	*Canadian Geotechnical Journal*
Manuscript ID	cgj-2020-0623.R1
Manuscript Type:	Article
Date Submitted by the Author:	22-Jan-2021
Complete List of Authors:	Wang, Chunyan; Chongqing University Liu, Hanlong; Chongqing University, College of Civil Engineering Ding, Xuanming; Chongqing University, ; Wang, Chenglong; Chongqing University Ou, Qiang; Chongqing University
Keyword:	Coral sand, Silica sand, Horizontal load, Particle breakage, P-y curve
Is the invited manuscript for consideration in a Special Issue? :	Not applicable (regular submission)

Study on the horizontal bearing characteristics of pile foundation in coral sand

Chunyan Wang[1,2], Hanlong Liu[1,2*], Xuanming Ding[1,2], Wang Chenglong[1,2], Qiang Ou[1,2]

Chunyan Wang
Ph.D. Student, Key Laboratory of New Technology for Construction of Cities in Mountain Area, Chongqing University, College of Civil Engineering, Chongqing, 400045, China.
E-mail: wangchyanl@163.com

***Hanlong Liu (Corresponding Author)**
Professor, Ph.D, Key Laboratory of New Technology for Construction of Cities in Mountain Area, College of Civil Engineering, Chongqing University, 83 Shapingba North Street, Chongqing, 400045, China.
*Corresponding Author, E-mail: hliuhhu@163.com

Xuanming Ding
Professor, Ph.D., Key Laboratory of New Technology for Construction of Cities in Mountain Area, Chongqing University, College of Civil Engineering, Chongqing, 400045, China.
E-mail: dxmhhu@163.com

Chenglong Wang
Research Fellow, Ph.D., Key Laboratory of New Technology for Construction of Cities in Mountain Area, Chongqing University, College of Civil Engineering, Chongqing, 400045, China.
E-mail: wangclong@cqu.edu.cn

Qiang Ou
Research Fellow, Ph.D., Key Laboratory of New Technology for Construction of Cities in Mountain Area, Chongqing University, College of Civil Engineering, Chongqing, 400045, China.
E-mail: ouq126@cqu.edu.cn

Abstract: This paper presents the horizontal bearing characteristics of piles in coral sand and silica sand from comparative experimental studies. A total of 6 model piles with different diameters are tested. The horizontal bearing capacity, deformation characteristic, bending moment, *p-y* curve, the change in soil horizontal pressure, as well as the particle breakage behaviour of coral sand are investigated. The results show that, in coral sand foundation, the horizontal bearing capacities of piles and the increments of soil horizontal pressures are obviously greater than those in silica sand. Accordingly, the lateral displacement, the rotation of pile head, the bending moment and the corresponding distribution depth in coral sand are significantly smaller than that in silica sand. The *p-y* curves indicate that the horizontal stiffness of coral sand is greater than that of silica sand. Remarkably, the breakage behaviour of coral sand is mainly distributed in the range of 10 times pile diameter depth and 5 times pile diameter width on the side where the sand is squeezed by pile. Furthermore, in coral sand, the influence of pile size is more pronounced, the squeezing force generated by pile spread farther and its influence range is larger compared to those in silica sand.

Key words: Coral sand, Silica sand, Horizontal load, Particle breakage, *P-y* curve.

Introduction

In recent years, with the increasing exploitation of oil, wind and gas resources, the construction projects of marine structures are developing rapidly around the world, such as offshore wind turbines and offshore drilling platforms. In these offshore engineering, the lateral loads, result from waves, winds, etc., are primarily born by pile foundations (Bhattacharya et al. 2013; Ding et al. 2021; Luan et al. 2020b). Noting that, on a global scale, the coral sand is distributed widely between 30°S and 30°N, such as the South China Sea and the Australia Sea, and the problems of coral sand sediment will inevitably be encountered. Therefore, in the design and construction of offshore engineering, it is highlighted from a practical standpoint to understanding the horizontal bearing characteristics of piles in coral sand.

Numerous tests and engineering examples show that the bearing capacity of pile is mainly determined by the properties of soil (Ding et al. 2020a). By investigating the micro-structures and the basic engineering properties of coral sand, the mechanical properties of coral sand are found to be significantly different from those of general continental and marine sediments (Luan et al. 2020a; Lv et al. 2019a; Lv et al. 2017). The coral sand is characterized by irregular shape, low unit weight, easily cemented, high porosity and large permeability, etc. (Konrad and Salami 2018; Ma et al. 2019; Zhu et al. 2016). Particularly, the coral sand particles are easy to break and disintegrate as compared with siliceous particles, which greatly affects the mechanical behaviour of coral sand (Coop and Atkinson 1994; Leung et al. 1996; Peng et al. 2019; Peng et al. 2020; Xiao and Liu 2017; Yu 2017). These small grains from the fractures and separation of protogenetic sand could fill the void space among particles, resulting in volumetric deformation and shrink under high pressures (Konrad and Salami 2018; Lee and Farhoomand 1967; Lv et al. 2019a). Significantly, the dilation phenomenon could be observed in coral sand at low confining pressure, which is different from silica sand (Miao and Airey 2013; Xiao et al. 2017; Zhang et al. 2015). Therefore, the design method of pile in the conventional foundation is not applicable in coral sand.

Up to now, a number of experimental and theoretical researches on the horizontal bearing characteristics of piles in silica sand (Guo 2006, 2013; Lin et al. 2015; Matlock 1970; Reese et al. 1974) and clay (Cecconi et al. 2019; Ding et al. 2020b; Hong et al. 2017; Huang et al. 2017) have been conducted, but the data concerning the coral materials is very limited (Dyson and Randolph 2001; Guo and Zhu 2005; Novello 1999; Wesselink et al. 1988; Williams et al. 1988). Nevertheless, the unique mechanical properties of coral sand have not been taken into account, and the derived load-transfer curves are not cast in a general form that would allow an extension to different conditions.

In view of above issues, a series of model pile tests in coral sand and silica sand are conducted in this study, aiming to reveal the lateral bearing characteristics of pile in coral sand. The lateral displacement and bending moment of pile are measured by means of displacement transducers and closed-spaced strain gauges. Besides, the changes in soil horizontal pressures and the particle breakage behaviour of coral sand are carefully measured and calculated. Furthermore, the *p-y* curves in coral sand and silica sand are discussed.

Overview of the experimental model

Model piles

In order to better simulate the pile-soil interaction in actual engineering, prefabricated reinforced concrete piles are employed in present study, and the detailed parameters are tabulated in Table 1. The pile diameters are 35 mm, 45 mm and 55 mm, respectively (Luan et al. 2020b). The same reinforcing cages composed of four straight steel wires and three stirrups with the same diameter of 2.6 mm are set in all model piles, and the thickness of protective layer is 5 mm. The measured bending stiffness of model pile is 2.73 $\mathrm{kN \cdot m^2}$, 5.33 $\mathrm{kN \cdot m^2}$ and 9.68 $\mathrm{kN \cdot m^2}$ respectively.

Sand

In this study, the coral sand is brought from the South China Sea, and the silica sand is the Fujian standard sand that is commonly used in engineering. Fig. 1(a) shows the initial grading of the adopted coral sand and silica sand with the same mean particle diameter (D_{50}=0.6). In addition, the shear behaviours of the sand used in this study are presented in Fig. 1(b) by the ring shear test. It is clear that the shear strength of coral sand is greater than that of silica sand, and the friction angle is 32° and 42°, respectively. Besides, the scanning electron micrographs of the sand used in this study are presented in Fig. 1(c-d). The intro-particle voids could be obviously observed in coral sand, indicating that this material possesses a high void ratio and crushable characteristics. The median values of flatness ratio, elongation ratio, convexity and angularity index of silica sand are 0.36, 0.34, 0.71 and 0.53 respectively, and these values of coral sand are 0.78, 0.45, 0.45 and 0.28 respectively (Bagheri et al. 2015; Blott and Pye 2007;

Kong and Fonseca 2018; Xiao et al. 2019). These morphology parameters exhibit that the silica sand is relatively round and its surface is smooth. In contrast, the particle shape of this coral sand is angular and its surface is rough. All other relevant mechanical parameters are provided in Table 2.

Testing equipment

Fig. 2 and Fig. 3 show the arrangement of experimental instruments and devices, which are composed of sand container, lateral loading system, measuring instrument and data acquisition system. The applied lateral load, pile head rotation, the lateral displacement of pile, bending moment, soil horizontal pressure and particle breakage of coral sand are carefully measured, respectively.

The sand container used in present study is locally manufactured by 12 mm thick organic glass and section steel with an internal dimension of 1 m (length) × 0.8 m (width) ×0.8 m (depth). The model piles are installed in the center of the sand container prior to sand. Then, 8 sand layers are prepared by the dry pluvial deposition method (Ganju et al. 2020; Ng et al. 2015; Zhu et al. 2019) to achieve a relative density of 40%. In order to facilitate the application of lateral load and the arrangement of measuring instruments, the top of the model piles is 150 mm higher than sand surface. Therefore, the effective embedded length of pile is shortened to 700 mm.

Horizontal load is applied to the installed model pile at ground elevation. The lateral loading system is formed by a fixed pulley, wire rope, counterweight blocks and other devices. The loading method is the slow load maintenance method with the load classification of 0.1 kN .

The measuring system used in this test consists of strain gauge, linear variable differential transformer (LVDT) and earth pressure cell. 24 strain gauges are symmetrically attached to the pile at two opposite sides, and keep a fixed interval of 50 mm along the pile embedded length. Six LVDTs are adopted to measure the lateral displacements of pile. Two of them are installed above the sand surface, one is placed at the loading position, and another one is placed at the position where is 100 mm above the sand surface. The rotation of pile head could be calculated by the difference between these two measured displacements. The remaining four LVDTs are connected to four rigid thin wires fixed at the measurement points through thin steel pipes and fixed pulleys, to measure the displacements of pile below the sand surface. These measuring points have a fixed interval of 150 mm along the pile embedded depth. Furthermore, 42 earth pressure cells are placed in sand with an interval 100 mm in the horizontal and vertical directions to measure the change in soil horizontal pressure, and the stress surface of cell is arranged vertically and facing the pile. In order to avoid the measurement error and ensure its reliability, the earth pressure cells are calibrated by the testing apparatus of one-dimensional compression prior to testing. The coral sand and silica sand used in this test are used to make the sand sample of one-dimensional compression test. The earth pressure cell is horizontally placed in the middle of the sand sample, which ensures the stress surface of the pressure sensor in good contact with the sand. The earth pressure cells can be well calibrated by comparing the vertical pressure applied on the sand sample and the value measured by the sensor. All measuring instruments are balanced (zeroed) before the load is applied, and all readings are simultaneously recorded by a multichannel data logger.

Coral sand is a kind of granular materials that is easy to break (Konrad and Salami 2018). Most of the existing indexes for quantitatively evaluating the crushability of granular materials are obtained by comparing the gradation curves before and after the particles crushing (Einav 2007; Hardin 1985; Peng et al. 2019; Xiao et al. 2016). The measure range of particle breakage behaviour is clearly shown in Fig. 2, and 140 sand samples are collected at an interval of 50 mm after the loading is completed. The obtained soil samples are sieved again to obtain the current gradation curves of coral sand.

Results and analysis

Horizontal bearing capacities of piles

An ultimate criterion proposed by Byrne et al. (2015) is defined by the minimum load level at either a ground level lateral displacement of 10%*D* or a ground level rotation of 2 °, where *D* is the diameter of model pile. Fig. 4(a) and Fig. 4(b) show the pile lateral displacement (at loading position) and the pile head rotation, respectively. The work-hardening behaviour can be clearly observed, implying that the pile foundation is still capable of bearing further lateral load even at a considerably large displacement of 10%*D* (Zhu et al. 2019). Fig. 4(c) summarizes the applied lateral load and the corresponding pile head rotation when the displacements at ground level reach 10%*D*. Noting that the ground level rotations are still less than 2° when the lateral displacements at ground elevate reach 10%*D*. Therefore, the corresponding load when the lateral displacement at ground level reaches 10%*D* is defined as the horizontal bearing capacity of pile.

It is worth noting that the horizontal bearing capacities of piles in coral sand are obviously higher than those in silica sand. For example, the bearing capacities of piles in coral sand are 0.47 kN (C35), 0.58 kN (C45) and 0.77 kN (C55), which are respectively 1.24 times, 1.29 times and 1.38 times of those in silica sand. Remarkably, the differences between the pile bearing capacities in coral sand and silica sand increase with the increase of pile diameter. This may be attributed to two respects: one is the irregular shape and rough surface of the coral sand can result in the stress dilatancy at low confining pressures, which can significantly improve the resistance to mutual movement between particles; and the other is the fine particles generated by particles crushing in coral sand can raise its compressive capacity by filling the void space.

Besides, the bearing capacities of piles, to a certain extent, increase by decreasing the length-diameter ratio. Especially in coral sand, the improvement of the bearing capacity caused by increasing pile diameter is more significant. For instance, when the diameter increases from 35 mm to 45 mm and 55 mm, the bearing capacity increases by 23.4% and 63.8% in coral sand, while the bearing capacity only increases by 18.4% and 47.4% in silica sand, respectively. This indicates that, in coral sand foundation, the bearing capacity of pile is more sensitive to the change in pile size than that of pile in silica sand. The improvement caused by increasing pile diameter in coral sand possibly results from two aspects: one is the bending stiffness of pile increases by increasing diameter, which is similar to the pile in silica sand. The other one is, the sand range squeezed by pile increases with the increase of diameter, resulting in the effects of stress dilatancy and the improvement of compressive stiffness caused by particle crushing behaviour of coral sand are more significant, which is unique to coral sand.

Lateral displacements of piles

The lateral displacements along pile depth under different loading levels (0.3 kN and 0.6 kN) are shown in Fig. 5. It is obvious that the lateral displacements mainly take place in the upper part of the piles, and show an increasing trend as the diameters decrease. The depth range, where the lateral displacements of piles mainly take place, increases with the increase of diameter under a relatively high loading level. For example, when the applied load is 0.6 kN, the lateral displacements of model piles with diameters 35 mm and 45 mm mainly occur within the depth of about 0.3 m. It is close to 0 at the lower part of pile, showing the characteristics of elastic long pile. When the diameter increases to 55mm, the displacements could be clearly observed in the entire depth of pile, illustrating that the sand around the pile is mobilized to resist external load in the entire depth range of pile. Noting that a slight reverse displacement can be observed near the pile bottom. The main reason may be the slight rigid rotation caused by the large bending stiffness in C55. Moreover, under the same loading level, the lateral displacements of piles in coral sand are significantly smaller than those in silica sand. At ground level, the average lateral displacement of piles in coral sand is approximately 52% of that in silica sand. This can be explained by that, the irregular shape and rough surface of coral sand can increase the resistance to mutual movement between particles, which can improve its ability to resist the development of pile displacement.

Fig. 6(a) shows the rotation angle of pile head at different loading levels. Obviously, the rotation of pile head exhibits a decreasing trend by increasing the pile diameter, resulting from the greater bending stiffness and pile-soil contact area of large-diameter pile. Moreover, the rotation of pile in coral sand is significantly smaller than that in silica sand, indicating that the inclination of the superstructure caused by pile deformation in coral sand is significantly smaller than that in silica sand. In addition, the rotation of pile head increases with the applied load, but the increment of pile rotation in coral sand is smaller than that in silica sand. For instance, when the applied lateral load is 0.3 kN, the pile head rotations in coral sand are 0.37°, 0.2° and 0.13°, which are smaller than those in silica sand (0.52°, 0.35° and 0.28°), respectively. When the applied load increases to 0.6 kN, the pile head rotations increase to 1.11°, 0.62° and 0.45° in coral sand, which are about 3 times of those at load level of 0.3 kN. Meanwhile, the pile rotations in silica sand also increase to 3.96 times (2.06°), 4.11 times (1.44°) and 3.43 times (0.96°) of those at load level of 0.3 kN respectively, which are significantly larger than those of piles in coral sand. Fig. 6(b) shows that, when the lateral displacements of all piles reach the same value at ground level, the displacement along the pile depth in coral sand is obviously smaller than that of the pile in silica sand.

Bending moment distribution on pile shaft

By attaching strain gauges symmetrically to pile at two opposite sides, the changes in tensile and compressive strains over the embedded length of pile could be carefully monitored. According to Eq. 1, the bending moment of model pile can be calculated, as shown in Fig. 7.

$$M = EI\Delta\varepsilon / D \tag{1}$$

where $\Delta\varepsilon$ is the difference between the tensile strain and the compressive strain of each section; D is the diameter of model pile; EI is the bending stiffness of model pile.

Fig. 7 shows the failure mode of the model pile and the distribution of the bending moment along pile depth. All model piles exhibit fracture failure finally, and the cracks are close to the depth associated with the maximum bending moment, which confirms the accuracy of measurement and the rationality of the calculation method of bending moment. The magnitudes and distribution areas of bending moment gradually increase with the lateral load. The reverse bending points, where the bending moment is equal to 0, always appear in the lower part of model piles and gradually move downward. This indicates that the depth ranges, where the piles mainly undergo bending deformation, gradually increase with the applied load. Also noting that, the value of the bending moment below the reverse bending point is rather small, showing the characteristics of flexible pile.

Fig. 8 shows the comparison of bending moment of mode piles with different diameters and sediment materials under the same loading level (0.3 kN). The changes in sediment material and pile diameter greatly influence the distribution of bending moment, as shown in Table 3. As the pile diameter increases, the magnitudes of bending moment decrease, while the distribution areas increase obviously. Meanwhile, the positions associated with the maximum bending moment, the reverse bending point and the crack move downward, demonstrating that a larger range of sand would be mobilized to resist the pile deformation, and a longer pile length would be mobilized to generate bending deformation to resist the applied external load. However, the small-diameter pile with small bending stiffness would take place more significant deformation, but its deformation just occurs in a small range. For example, when the applied lateral load is 0.3 kN, the corresponding depth of the maximum bending moment

(153.32 $\mathrm{N \cdot M}$) is 0.14 m below the sand surface in C35. With the increasing of pile diameters, the maximum bending moment decrease by 14.4% and 20.9% to 131.28 $\mathrm{N \cdot M}$ and 121.14 $\mathrm{N \cdot M}$, respectively. Meanwhile, the position associated with the maximum bending moment moves downward to -0.20 m and -0.26 m, and the depth of crack also moves downward to 0.17 m and 0.28 m, respectively.

When the sediment material is replaced to silica sand, the similar rule discussed above can be obtained. However, in silica sand, the magnitudes and the distribution depths of bending moments are significantly greater than those in coral sand. Therefore, the required pile length mobilized to generate bending deformation for resisting external load would become longer. Meanwhile, the sand ranges mobilized to resist the pile deformation would also become larger. In addition, the increment of bending moment in silica sand induced by increasing the pile diameter is not as significant as that in coral sand. For example, the maximum bending moments of piles are 213.96 $\mathrm{N \cdot M}$, 188.86 $\mathrm{N \cdot M}$ and 175.03 $\mathrm{N \cdot M}$ in silica sand respectively, which are greater than those in coral sand. When the diameter increases from 35 mm to 45 mm and 55 mm, the maximum bending moment only decreases by 11.7% and 18.2% in silica sand respectively, which is less than the decrement in coral sand (14.4% and 20.9%). This implies that the influence of pile size on the bending moment is more significant in coral sand than that in silica sand.

Soil-pile interaction force-displacement relationships (*p-y* curves)

The primary method used to obtain the load transfer curves (*p-y* curves), for this study, is based on the manipulation of recorded experimental bending moment data (Dyson and Randolph 2001; Lin et al. 2015; Suits et al. 2007; Wesselink et al. 1988). According to Dyson and Randolph (2001), the experimental bending-moment data are fitted with two polynomials using the least-squares technique, then spliced the two polynomials together using the boundary conditions of the continuity of shear force and force per unit length as well as zero pile tip moment. The soil-pile interaction force per unit length *P* is obtained by double differentiating the bending moment profile, and the lateral displacements *y* is calculated by double integrating the curvature *M/EI*. It is well-known that double differentiation is very sensitive to data noise. Up to now, several techniques have been proposed to minimize numerical errors due to double differentiation (Dou and Byrne 2011; Dyson and Randolph 2001; Reese et al. 1975). In order to further minimize the influence of data noise on double differentiation, the authors improve the method proposed by Dyson and Randolph (2001) by fitting the experimental bending moment data below the soil surface with five-order polynomials rather than four-order polynomials. In this study, four horizontal displacement monitoring points are arranged along the pile length below the sand surface, as shown in Fig. 2. Therefore, the four measured lateral displacements below the sand surface are also taken as the boundary condition to modify the fitting parameters so as to reduce the data noise. The pile deformation is very small below -0.2 m (see Figs. 5 and 6), therefore, only the pile-soil interaction relationship above -0.2 m is discussed.

$$p = \frac{\mathrm{d}^2 M}{\mathrm{d}z^2} \tag{2}$$

$$y = \iint \frac{M}{EI} \mathrm{d}z^2 \tag{3}$$

The *p-y* curves at serval depths along the pile length are presented in Fig. 9. It should be pointed out that the last numerals in the legend denote the depth below soil surface. As expected, the *p-y* curves have a general trend of increasing initial slope (initial stiffness) and ultimate soil reaction as the depth and diameter increase. Noting that the soil-pile interaction force P in coral sand is larger than that in silica sand under the same lateral displacement *y*, indicating the horizontal stiffness of coral sand is greater than that of silica sand foundation.

This can well explain the previous conclusion that, the horizontal bearing capacity of pile in coral sand is obviously greater than that in silica sand foundation, from the perspective of mechanical mechanism.

Increase in soil horizontal pressure around pile

During the test, the change in soil horizontal pressure near the pile is measured by the in-soil null pressure sensors, which are placed in the soil during the sand-raining process and arranged at an equal interval along the load applied direction. The measuring width is 400mm (the 100mm on the left of pile plus the 300mm on the right of pile) and the measuring depth is the entire embedment depth of pile (in Fig. 2). The measurements of each in-soil pressure sensor then are used to generate contours, to show the change in soil horizontal pressure at each loading step.

The lateral displacement of the pile at ground level is an important index to determine the bearing characteristics. When the ground level displacements of all model piles reach the critical displacement (10%*D*), the changes in soil horizontal pressures within the measuring ranges are shown in Fig. 10 and Fig. 11. Noting that, the positive numbers in the legend represent the increment of soil horizontal pressure, and negative numbers represent the decrement of soil horizontal pressure. The horizontal soil pressure illustrates a significant increasing trend in the upper right part of the sand. On the right side of pile, the soil horizontal pressure initially increases and then shows a decreasing trend along the depth. On the left side of pile, some slight increments can be observed near the pile bottom due to the pile's reverse displacement at the lower part, more details are shown in Table 4.

As the pile diameter increases, the maximum increment and the change zone of soil horizontal pressures increase dramatically, and the depth associated with the maximum increment also moves downward. In test C35, the maximum increment of soil pressure is 36.88 kPa at the depth of -0.17 m. By increasing the pile diameter to 45 mm and 55 mm, the maximum increments of soil pressure in coral sand increase to 75.49 kPa and 127.81 kPa, which are approximately 2.05 times and 3.47 times of that in C35, respectively. The point corresponding to the maximum increments also moves down to -0.23 m and -0.26 m, respectively. Significantly, farther away from the pile, the smaller the changes in soil horizontal pressures. Taking the vertical plane about 0.3 m away from the right side of the pile as an example, the maximum increment of soil horizontal pressure reduces by 85.87% from 36.88 kPa to 5.26 kPa in C35. The decrements are 78.35% in C45 and 73.44% in C55, which are smaller than that in C35, indicating that the soil horizontal pressure produced by the squeeze action of pile spreads farther when the diameter increases.

Remarkably, the influence of sediment material on the change in soil horizontal pressure also cannot be ignored. In coral sand, the increments of soil horizontal pressure are much larger than those in silica sand, but the influence of pile diameter is more significant than that in silica sand. For instance, the maximum increments of soil horizontal pressures in silica sand are only 26.72 kPa, 46.84 kPa and 70.61 kPa, which are obviously smaller than those in coral sand, respectively. When the pile diameter increases, the maximum increments in S45 and S55 are only 1.75 times and 2.64 times of that in S35, which are still smaller than the increases caused by changing the pile diameter in coral sand (2.05 times and 3.47 times). This phenomenon can be explained by the stress dilatancy of coral sand at low confining pressures, indicating that the change in soil horizontal pressure in coral sand is more sensitive to the variation of pile diameter. Moreover, in the vertical plane where 0.3 m away from the right side of the pile, the maximum increments of soil horizontal pressures reduce by 90.4% (S35), 87.0% (S45) and 80.8% (S55) in silica sand respectively, which are greater than that in coral sand, implying that the squeezing force generated by the pile spreads farther and has a larger influence range in coral sand.

Particle breakage distribution in coral sand

The bearing capacity of the pile is mainly determined by the properties of the soil. In nature, the soil is usually composed of granular materials and will display crushing behaviour under considerable stress. To date, there are many kinds of indexes can quantify the particle breakage characteristics of granular particles. Among them, the particle breakage indexes proposed by Hardin (1985) and Einav (2007) are most widely used. The main difference between the two methods is the definition of the breakage potential (B_p). Accordingly, the ratio of Hardin's particle breakage index (B_r) to that of Einav is equal to the ratio of Einav' breakage potential (B_p) to that of Hardin. No matter whether the method proposed by Hardin (1985) or Einav (2007) is used, the distribution and level of breakage around the laterally loaded piles are not affected. Since the model proposed by Einav is affected by the value of the fractal dimension of coral sand, the Hardin's relative particle breakage index (expressed as Eq. 4) is adopted in this study, as shown in Fig. 12.

$$B_r = B_t / B_p \tag{4}$$

where B_r is the particle breakage index; B_t is the total breakage, expressed by the area surrounded by the particle size line of 0.074 mm, the initial gradation curve and the current gradation curve; B_p is the breakage potential, expressed by the area surrounded by the particle size line of 0.074 mm and the initial grading.

After the loading is completed, the sand samples selected at the same intervals are sieved by geo-sieve to obtain the particle gradation curves. By substituting the particle gradation curves of each measurement point before and after testing into Hardin's relative breakage index model, the distribution of particle breakage behaviour could be obtained. Due to the fact that the silica sand is not easy to break at the low earth pressure and its influence is negligible (Lv et al. 2019b; Lv et al. 2017; Xiao et al. 2018), the particle breakage of the silica sand is not measured in this experiment. The distributions of particle breakage indexes are shown in Fig. 13, which are similar to the distribution of the change in soil horizontal pressure.

In coral sand, the breakage behaviour is mainly distributed in the sand range of 10 times pile diameter depth and 5 times pile diameter width on the right side of pile. The degree and distribution range of particle breaking behaviour increase significantly when the pile diameter increases. It clearly shows that the particle breakage behaviour on right side of the pile is very significant in C55, and the sand zone with the relative breakage index B_r greater than 0.8% is mainly distributed in the depth range from -0.07 m to -0.50 m and the width is 0.25 m. Even in the sand range where is 0.30 m away from the pile, the particle breakage phenomenon can still be measured. On the left side of pile in C55, the particle breakage behaviour is not obvious, and it only occurs below the depth of -0.4 m. When the pile diameter is 45 mm, the sand zone, where the relative breakage index B_r is greater than 0.8%, is reduced by half, as compared to C55. Noting that the degree and distribution of particle breakage in C35 are very small, indicating that the improvement of the bearing capacity in C35 resulted from the particle crushing behaviour is negligible. Therefore, the relatively high horizontal bearing capacity of C35 (as compared to S35) is mainly caused by the stress dilatancy and the large mutual sliding friction resistance of coral sand.

5 Conclusions

This paper presents an experimental study on the horizontal bearing characteristics of pile in coral sand and silica sand, which could lay a great reference for further theoretical and experimental study of pile-soil interaction in coral sand. These key experimental findings are summarized as follows:

(1) The lateral bearing capacity of pile in coral sand is obviously greater than that in silica sand, and the improvement of bearing capacity caused by increasing pile diameter is more significant in coral sand. Furthermore, the soil-pile interaction force in coral sand is greater than that in silica sand through the calculated *p-y* curve, indicating that the horizontal stiffness of coral sand is greater than that of silica sand.

(2) The lateral displacements of pile and the pile head rotations in coral sand are significantly smaller than those in silica sand. Moreover, in coral sand, the pile displacement is more sensitive to the change in pile sizes, and the pile head rotation is more insensitive to the applied load, as compared to the pile in silica sand foundation.

(3) All model piles exhibit fracture failure and show the characteristics of flexible pile. The

bending moments and corresponding distribution depth in silica sand are larger than those in coral sand. Besides, the bending moments show a decreasing trend as the pile diameter increases, and the variation of bending moment induced by the pile diameter in coral sand is more significant than that in silica sand.

(4) The increment of soil horizontal pressure caused by the squeezing action of pile in coral sand is much greater than that in silica sand, and shows an increasing trend by increasing the pile diameter. Significantly, in coral sand foundation, the influence of pile size is more pronounced, and the squeezing force generated by the pile spreads farther and its influence range is larger, as compared to silica sand foundation.

(5) The breakage behaviour is mainly distributed in the sand range of 10 times pile diameter depth and 5 times pile diameter width along the load applied direction. Remarkably, the distribution and level of breakage are affected greatly by the pile diameter. As the pile diameter increases, the particle crushing behaviour become more obvious, and the effect on the bearing capacity of pile cannot be ignored.

Acknowledgments

This work is supported by the National Natural Science Foundation of China (Grant Nos. 41831282 and 51878103) and Innovation Group Science Foundation of the Natural Science Foundation of Chongqing, China (Grant No.cstc2020jcyj-cxttX0003).

References

Bagheri, G.H., Bonadonna, C., Manzella, I., and Vonlanthen, P. 2015. On the characterization of size and shape of irregular particles. Powder Technology, **270**: 141-153. doi:10.1016/j.powtec.2014.10.015.

Bhattacharya, S., Nikitas, N., Garnsey, J., Alexander, N.A., Cox, J., Lombardi, D., Muir Wood, D., and Nash, D.F.T. 2013. Observed dynamic soil–structure interaction in scale testing of offshore wind turbine foundations. Soil Dynamics and Earthquake Engineering, **54**: 47-60. doi:10.1016/j.soildyn.2013.07.012.

Blott, S.J., and Pye, K. 2007. Particle shape: a review and new methods of characterization and classification. Sedimentology, **0**(0): 070921092734002-??? doi:10.1111/j.1365-3091.2007.00892.x.

Byrne, B., Zdravković, L., Taborda, D., Potts, D., Jardine, R., Sideri, M., Schroeder, F., McAdam, R., Burd, H., Houlsby, G., Martin, C., Gavin, K., Doherty, P., Igoe, D., Wood, A., Kallehave, D., and Gretlund, J. 2015. Numerical modelling of large diameter piles under lateral loading for offshore wind applications. *In* Frontiers in Offshore Geotechnics III. pp. 759-764.

Cecconi, M., Pane, V., Vecchietti, A., and Bellavita, D. 2019. Horizontal capacity of single piles: an extension of Broms' theory for c-ϕ soils. Soils and Foundations. doi:10.1016/j.sandf.2019.01.007.

Coop, M., and Atkinson, J. 1994. Discussion: The mechanics of cemented carbonate sands. Géotechnique, **44**: 533-537. doi:10.1680/geot.1994.44.3.533.

Ding, X., Qu, L., Yang, J., and Wang, C. 2020a. Experimental study on the pile group-soil vibration induced by railway traffic under the inclined bedrock condition. Acta Geotechnica,(1–5).

Ding, X., Feng, L., Wang, C., Chen, Z., and Han, L. 2020b. Shaking table tests of the seismic response of a utility tunnel with a joint connection. Soil Dynamics and Earthquake Engineering, **133**(Jun.): 106133.106131-106133.106112.

Ding, X., Zhang, Y., Wu, Q., Chen, Z., and Wang, C. 2021. Shaking table tests on the seismic responses of underground structures in coral sand. Tunnelling and Underground Space Technology, **109**. doi:10.1016/j.tust.2020.103775.

Dou, H., and Byrne, P. 2011. Dynamic response of single piles and soil–pile interaction. Canadian Geotechnical Journal, **33**: 80-96. doi:10.1139/t96-025.

Dyson, G.J., and Randolph, M.F. 2001. Monotonic Lateral Loading of Piles in Calcareous Sand. Journal of Geotechnical and Geoenvironmental Engineering, **127**(4): 346-352. doi:doi:10.1061/(ASCE)1090-0241(2001)127:4(346).

Einav, I. 2007. Breakage mechanics—Part I: Theory. Journal of The Mechanics and Physics of Solids, **55**(6): 1274-1297. doi:10.1016/j.jmps.2006.11.003.

Ganju, E., Han, F., Prezzi, M., Salgado, R., and Pereira, J.S. 2020. Quantification of displacement and particle crushing around a penetrometer tip. Geoscience Frontiers, **11**(2): 389-399. doi:10.1016/j.gsf.2019.05.007.

Guo, W., and Zhu, B. 2005. Static and cyclic behavior of laterally loaded piles in calcareous sand. *In* Frontiers in Offshore Geotechnics.

Guo, W.D. 2006. On limiting force profile, slip depth and response of lateral piles. Computers and Geotechnics, **33**(1): 47-67. doi:10.1016/j.compgeo.2006.02.001.

Guo, W.D. 2013. Simple Model for Nonlinear Response of 52 Laterally Loaded Piles. Journal of Geotechnical and Geoenvironmental Engineering, **139**(2): 234-252. doi:doi:10.1061/(ASCE)GT.1943-5606.0000726.

Hardin, B.O. 1985. Crushing of Soil Particles. Journal of Geotechnical Engineering, **111**(10): 1177-1192.

Hong, Y., He, B., Wang, L.Z., Wang, Z., Ng, C.W.W., and Mašín, D. 2017. Cyclic lateral response and failure mechanisms of semi-rigid pile in soft clay: centrifuge tests and numerical modelling. Canadian Geotechnical Journal, **54**(6): 806-824. doi:10.1139/cgj-2016-0356.

Huang, M.S., Ma, H., Li, S., Yu, J., and Zhang, C.R. 2017. Static and cyclic p-y curves for laterally loaded piles in soft clay. Yantu Gongcheng Xuebao/Chinese Journal of Geotechnical Engineering, **39**: 9-12. doi:10.11779/CJGE2017S2003.

Kong, D., and Fonseca, J. 2018. Quantification of the morphology of shelly carbonate sands using 3D images. Géotechnique, **68**(3): 249-261. doi:10.1680/jgeot.16.P.278.

Konrad, J., and Salami, Y. 2018. Particle breakage in granular materials — a conceptual framework. Canadian Geotechnical Journal, **55**(5): 710-719. doi:10.1139/cgj-2017-0224.

Lee, K.L., and Farhoomand, I. 1967. Compressibility And Crushing Of Granular Soil In Anisotropic Triaxial Compression. Canadian Geotechnical Journal, **4**(1): 68-86. doi:10.1139/t67-012.

Leung, C.F., Lee, F.H., and Yet, N.S. 1996. The role of particle breakage in pile creep in sand. Canadian Geotechnical Journal, **33**(6): 888-898. doi:doi:10.1139/t96-119.

Lin, H., Ni, L., Suleiman, M.T., and Raich, A. 2015. Interaction between Laterally Loaded Pile and Surrounding Soil. Journal of Geotechnical and Geoenvironmental Engineering, **141**(4). doi:10.1061/(asce)gt.1943-5606.0001259.

Luan, L., Zheng, C., Kouretzis, G., and Ding, X. 2020a. Dynamic analysis of pile groups subjected to horizontal loads considering coupled pile-to-pile interaction. Computers and Geotechnics, **117**(Jan.): 103276.103271-103276.103278.

Luan, L., Ding, X., Zheng, C., Kouretzis, G., and Wu, Q. 2020b. Dynamic response of pile groups subjected to horizontal loads. Canadian Geotechnical Journal, **57**(4): 469-481. doi:org/10.1139/cgj-2019-0031.

Lv, Y., Liu, J., and Xiong, Z. 2019a. One-dimensional dynamic compressive behavior of dry calcareous sand at high strain rates. Journal of Rock Mechanics and Geotechnical Engineering, **11**(1): 192-201. doi:10.1016/j.jrmge.2018.04.013.

Lv, Y., Wang, Y., and Zuo, D. 2019b. Effects of particle size on dynamic constitutive relation and energy absorption of calcareous sand. Powder Technology, **356**: 21-30. doi:10.1016/j.powtec.2019.07.088.

Lv, Y., Li, F., Liu, Y., Fan, P., and Wang, M. 2017. Comparative study of coral sand and silica sand in creep under general stress states. Canadian Geotechnical Journal, **54**(11): 1601-1611. doi:10.1139/cgj-2016-0295.

Ma, L., Li, Z., Wang, M., Wei, H., and Fan, P. 2019. Effects of size and loading rate on the mechanical properties of single coral particles. Powder Technology, **342**: 961-971. doi:10.1016/j.powtec.2018.10.037.

Matlock, H. 1970. Correlation for Design of Laterally Loaded Piles in Soft Clay. Proc. 2nd Offshore Technology Conf., **1**. doi:10.4043/1204-MS.

Miao, G., and Airey, D. 2013. Breakage and ultimate states for a carbonate sand. Géotechnique, **63**(14): 1221-1229. doi:10.1680/geot.12.P.111.

Ng, C.W.W., Shi, J., Mašín, D., Sun, H., and Lei, G.H. 2015. Influence of sand density and retaining wall stiffness on three-dimensional responses of tunnel to basement excavation. Canadian Geotechnical Journal, **52**(11): 1811-1829. doi:10.1139/cgj-2014-0150.

Novello, E.A. 1999. From static to cyclic p-y data in calcareous sediments. *In* International conference on calcareous sediments (1988-03-15). A.A. Balkema, Rotterdam, Balkema, Rotterdam, The Netherlands, . pp. 17-27.

Peng, Y., Ding, X., Xiao, Y., Deng, X., and Deng, W. 2019. Detailed amount of particle breakage in non-uniformly graded sands under one-dimensional compression. Canadian Geotechnical Journal. doi:10.1139/cgj-2019-0283.

Peng, Y., Liu, H., Li, C., Ding, X., Deng, W., and Wang, C. 2020. The detailed particle breakage around the pile in coral sand. Acta Geotechnica.

Reese, L., Cox, W., and Koop, F. 1975. Field Testing and Analysis of Laterally Loaded Piles om Stiff Clay. Proc. 7th Offshore Technology Conf., **2**. doi:10.4043/2312-MS.

Reese, L.C., Cox, W.R., and Koop, F.D. 1974. Analysis of Laterally Loaded Piles in Sand. *In* Offshore Technology Conference. Offshore Technology Conference, Houston, Texas. p. 11.

Suits, L.D., Sheahan, T.C., Yang, K., and Liang, R. 2007. Methods for Deriving p-y Curves from Instrumented Lateral Load Tests. Geotechnical Testing Journal - GEOTECH TESTING J, **30**. doi:10.1520/GTJ100317.

Wesselink, B.D., Murff, J.D., Randolph, M.F., Nunez, I.L., and Hyden, A.M. 1988. Analysis of centrifuge model test data from laterrally loaded piles in calcareous sand; Analyse de données de modèle d'essai de centrifugation à partir de pieux chargés latéralement dans du sable calcaire. *In* International conference on calcareous sediments (1988-03-15). A.A. Balkema, Rotterdam, Balkema, Rotterdam, The Netherlands, . pp. 261-270.

Williams, A.F., Dunnavant, T.W., Anderson, S., Equid, D.W., and Hyden, A.M. 1988. The performance and analysis of lateral load tests on 356 mm dia piles in reconstituted calcareous sand; Caractéristiques et analyse d'essais de chargement latéral sur des pieux de 356 mm dans du sable calcaire reconstitué. *In* International conference on calcareous sediments (1988-03-15). A.A. Balkema, Rotterdam. pp. 271-280.

Xiao, Y., and Liu, H. 2017. Elastoplastic Constitutive Model for Rockfill Materials Considering Particle Breakage. International Journal of Geomechanics, **17**(1): 04016041. doi:10.1061/(ASCE)GM.1943-5622.0000681.

Xiao, Y., Liu, H., Xiao, P., and Xiang, J. 2016. Fractal crushing of carbonate sands under impact loading [Article]. Geotechnique Letters, **6**(3): 199-204. doi:10.1680/jgele.16.00056.

Xiao, Y., Yuan, Z., Lv, Y., Wang, L., and Liu, H. 2018. Fractal crushing of carbonate and quartz sands along the specimen height under impact loading. Construction and Building Materials, **182**: 188-199. doi:10.1016/j.conbuildmat.2018.06.112.

Xiao, Y., Long, L., Evans, T.M., Zhou, H., and Stuedlein, A.W. 2019. Effect of Particle Shape on Stress-Dilatancy Responses of Medium-Dense Sands. Journal of Geotechnical and Geoenvironmental Engineering, **145**(2): 04018105.

Xiao, Y., Liu, H., Chen, Q., Ma, Q., Xiang, Y., and Zheng, Y. 2017. Particle breakage and deformation of carbonate sands with wide range of densities during compression loading process. Acta Geotechnica, **12**(5): 1177-1184. doi:DOI: 10.1007/s11440-017-0580-y.

Yu, F.W. 2017. Particle breakage and the critical state of sands. Géotechnique, **67**(8): 713-719. doi:10.1680/jgeot.15.P.250.

Zhang, S., Tong, C.X., Li, X., and Sheng, D. 2015. A new method for studying the evolution of particle breakage. Géotechnique, **65**(11): 911-922. doi:10.1680/jgeot.14.P.240.

Zhu, B., Wen, K., Li, T., Wang, L., and Kong, D. 2019. Experimental study on lateral pile–soil interaction of offshore tetrapod piled jacket foundations in sand. Canadian Geotechnical Journal, **56**(11): 1680-1689. doi:10.1139/cgj-2018-0292.

Zhu, C., Liu, H., and Zhou, B. 2016. Micro-structures and the basic engineering properties of beach calcarenites in South China Sea. Ocean Engineering, **114**: 224-235. doi:10.1016/j.oceaneng.2016.01.009.

Tables

Table 1. Parameters of model piles

Test no.	Pile diameter (mm)	Pile length (mm)	Embedded pile length (mm)	Bending stiffness $(kN \cdot m^2)$	Number of strain gauges	Sediment material
C35	35	850	700	2.73	24	Coral sand
C45	45	850	700	5.33	24	
C55	55	850	700	9.68	24	
S35	35	850	700	2.73	24	Silica sand
S45	45	850	700	5.33	24	
S55	55	850	700	9.68	24	

Table 2. Sand Parameters

Property	Coral sand	Silica sand
Maximum dry density, $g_{\max}$: g/cm^3	1.62	1.69
Minimum dry density, $g_{\min}$: g/cm^3	1.22	1.56
Specific gravity, G_s	2.81	2.63
Mean particle diameter, D_{50}: mm	0.6	0.6

Table 3. Bending moment and crack location of piles

Test no.	C35	C45	C55	S35	S45	S55
Maximum bend moment at load level of 0.3 kN: N • M	153.32	131.28	121.14	213.96	188.86	175.03
Corresponding depth of maximum bending moment: m	-0.14	-0.20m	-0.26	-0.2	-0.26	-0.32
Depth of crack: m	-0.13	-0.17	-0.28	-0.16	-0.24	0.3
Depth of reverse bending points: m	-0.38	-0.46	-0.54	-0.43	-0.5	0.57

Table 4. Variation of the soil horizontal pressure

Test no.	C35	C45	C55	S35	S45	S55
the maximum increment of soil horizontal pressures, kPa	36.88	75.49	127.81	26.72	46.84	70.61
Depth of extreme point，m	-0.17	-0.23	-0.26	-0.22	-0.25	-0.25
the maximum increment of soil horizontal pressures where 0.3 m away from piles, kPa	5.26	16.34	33.94	2.56	6.09	10.67

Figure Captions

Figure 1. (a) Initial particle-size distributions; (b) Shear strength of silica sand and coral sand; (c) Scanning electron microscopy for silica sand; (d) Scanning electron microscopy for coral sand.

Figure 2. Arrangement of the experimental instruments: (a) Front view; (b) Vertical view.

Figure 3. Physical layout of the experimental instruments.

Figure 4. (a) Lateral load-displacement curves at loading position; (b) Lateral load-rotation curves; (c) Horizontal bearing capacities of model piles.

Figure 5. The lateral displacements of piles along depth at different load levels: (a) D=35 mm; (b) D=45 mm; (c) D=55 mm

Figure 6. (a) Rotation of pile head at different loading levels; (b) Lateral displacements along pile depth when the lateral displacements at ground level reach 10%D.

Figure 7. Distribution of bending moments of piles with different diameters; (a) C35; (b) C45; (c) C55; (d) S35; (e) S45; (f) S55.

Figure 8. The comparison of bending moment at loading level of 0.3 kN.

Figure 9. *P*-*y* curves at serval depths along the pile length: (a) *D*=35 mm; (b) *D*=45 mm; (c) *D*=55 mm.

Figure 10. The changes in soil horizontal pressures of coral sand foundation: (a) C35; (b) C45; (c) C55.

Figure 11. The changes in soil horizontal pressures of silica sand foundation: (a) S35; (b) S45; (c) S55.

Figure 12. Definition of relative breakage index.

Figure 13. The distribution and level of particle breakage around the laterally loaded piles in coral sand: (a) C55; (b) C45; (c) C35.

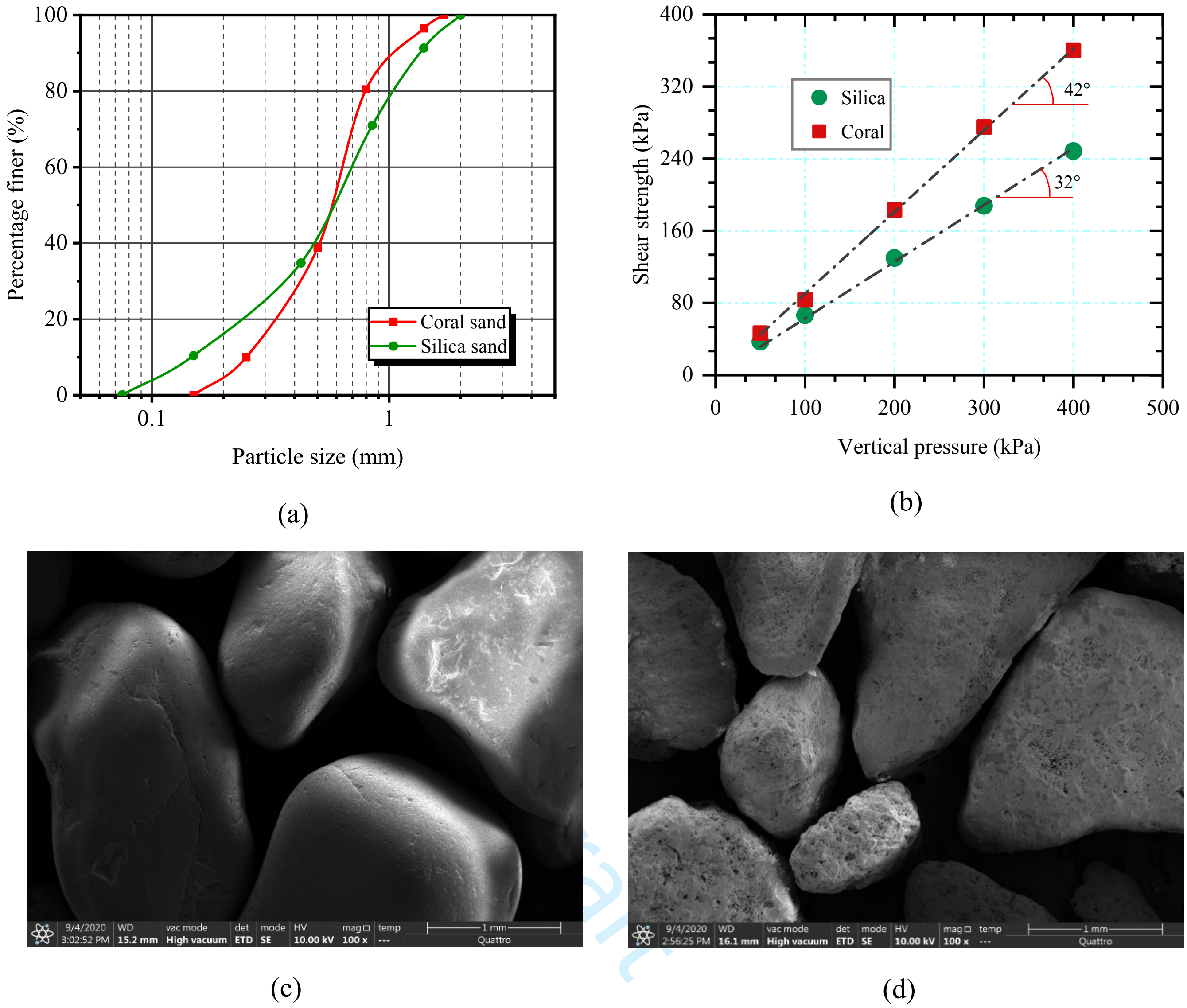

Figure 1. (a) Initial particle-size distributions; (b) Shear strength of silica sand and coral sand; (c) Scanning electron microscopy for silica sand; (d) Scanning electron microscopy for coral sand.

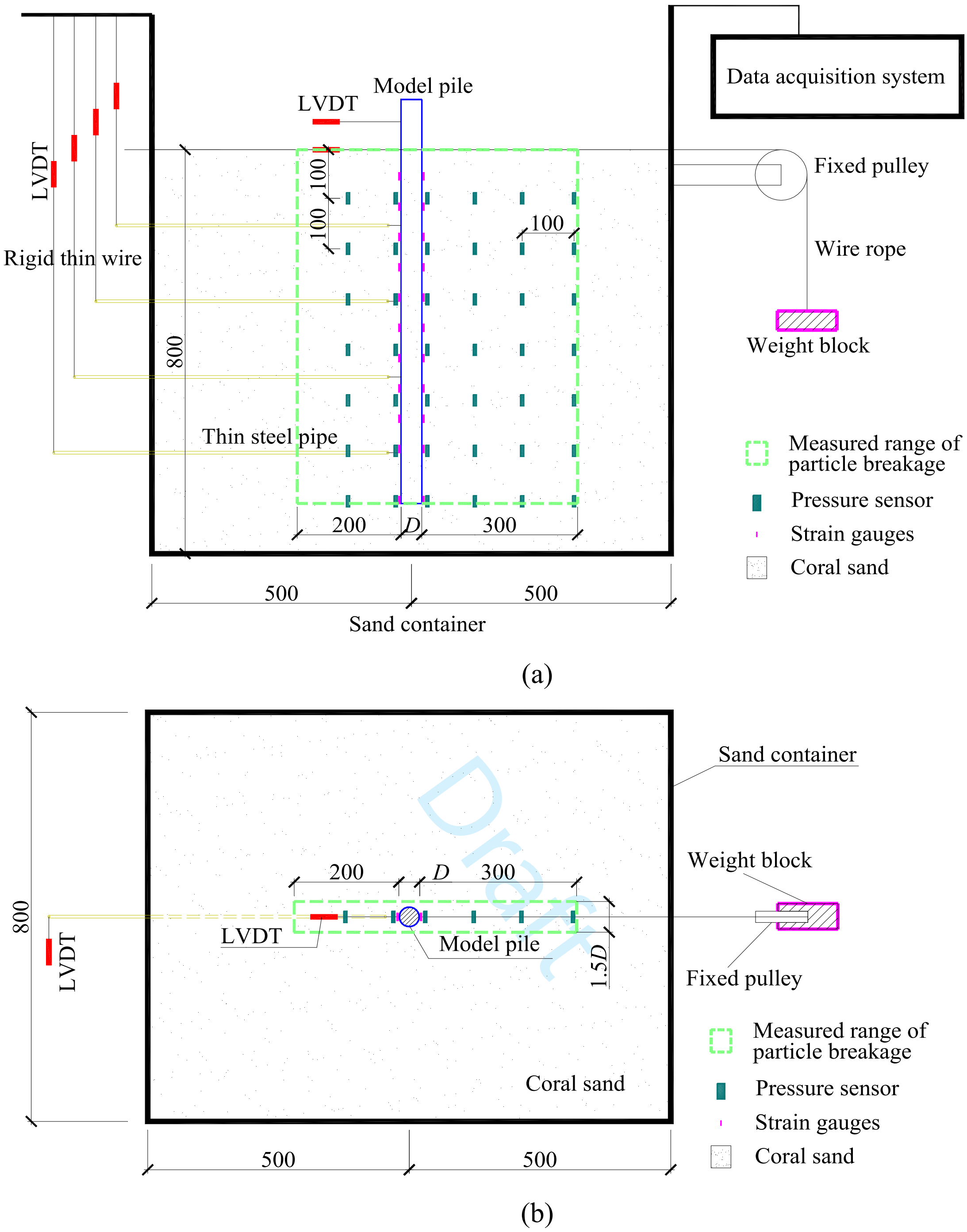

Figure 2. Arrangement of the experimental instruments: (a) Front view; (b) Vertical view

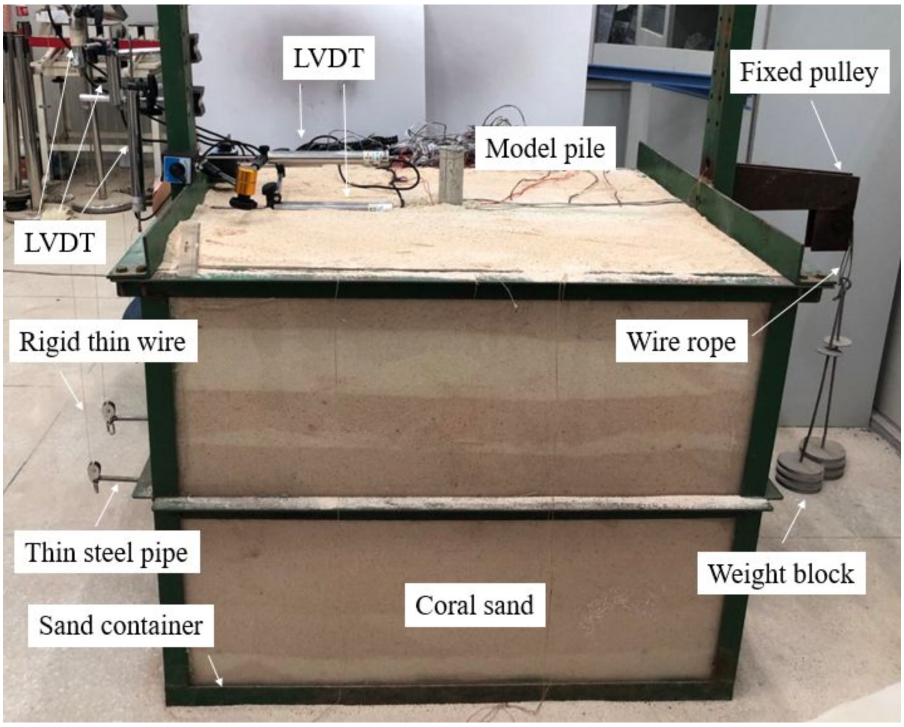

Figure 3. Physical layout of the experimental instruments.

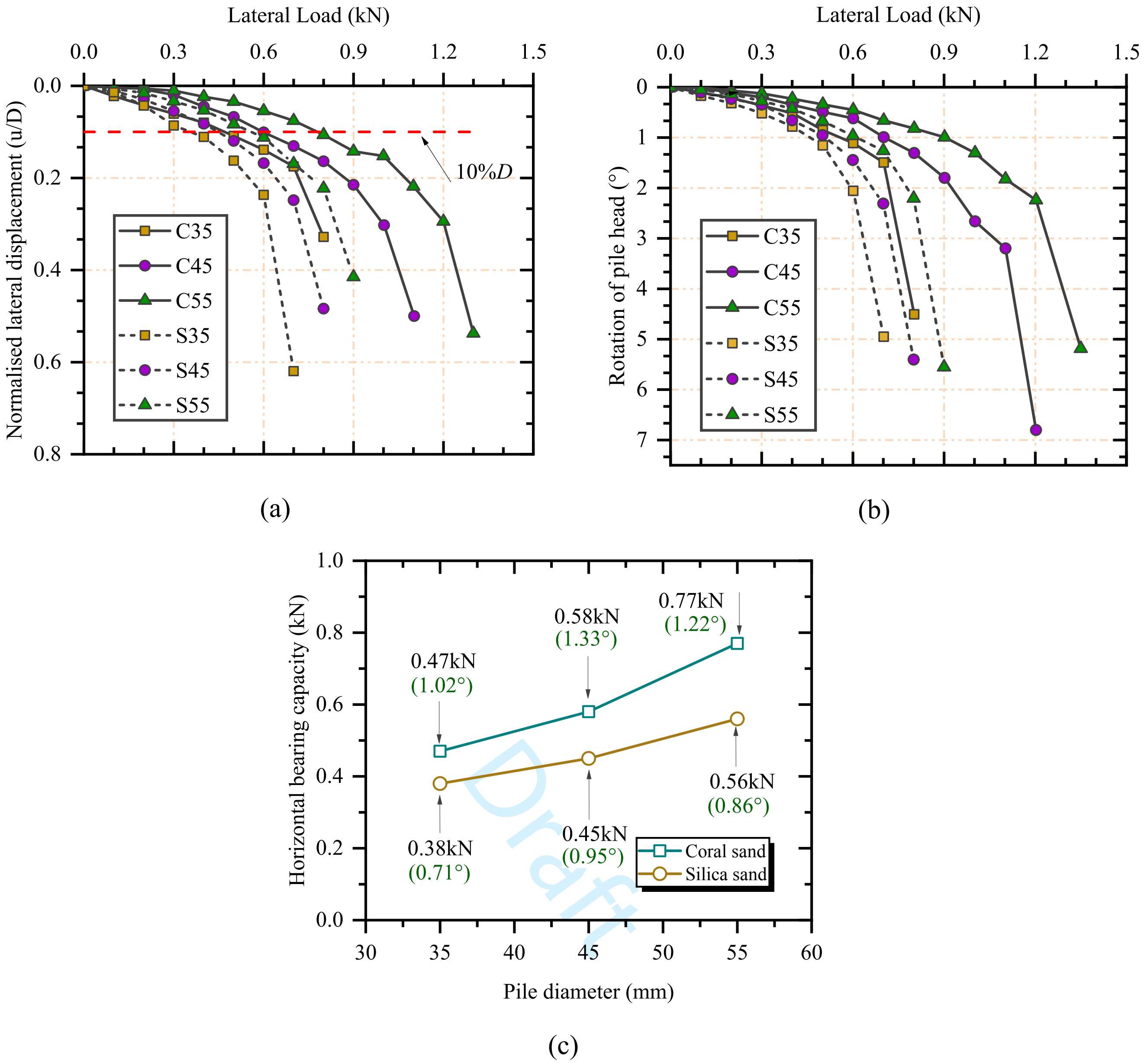

Figure 4. (a) Lateral load-displacement curves at loading position; (b) Lateral load-rotation curves; (c) Horizontal bearing capacities of model piles.

Note: The letter *u* means the lateral displacement of model pile at ground level and *D* is the diameter of model pile.

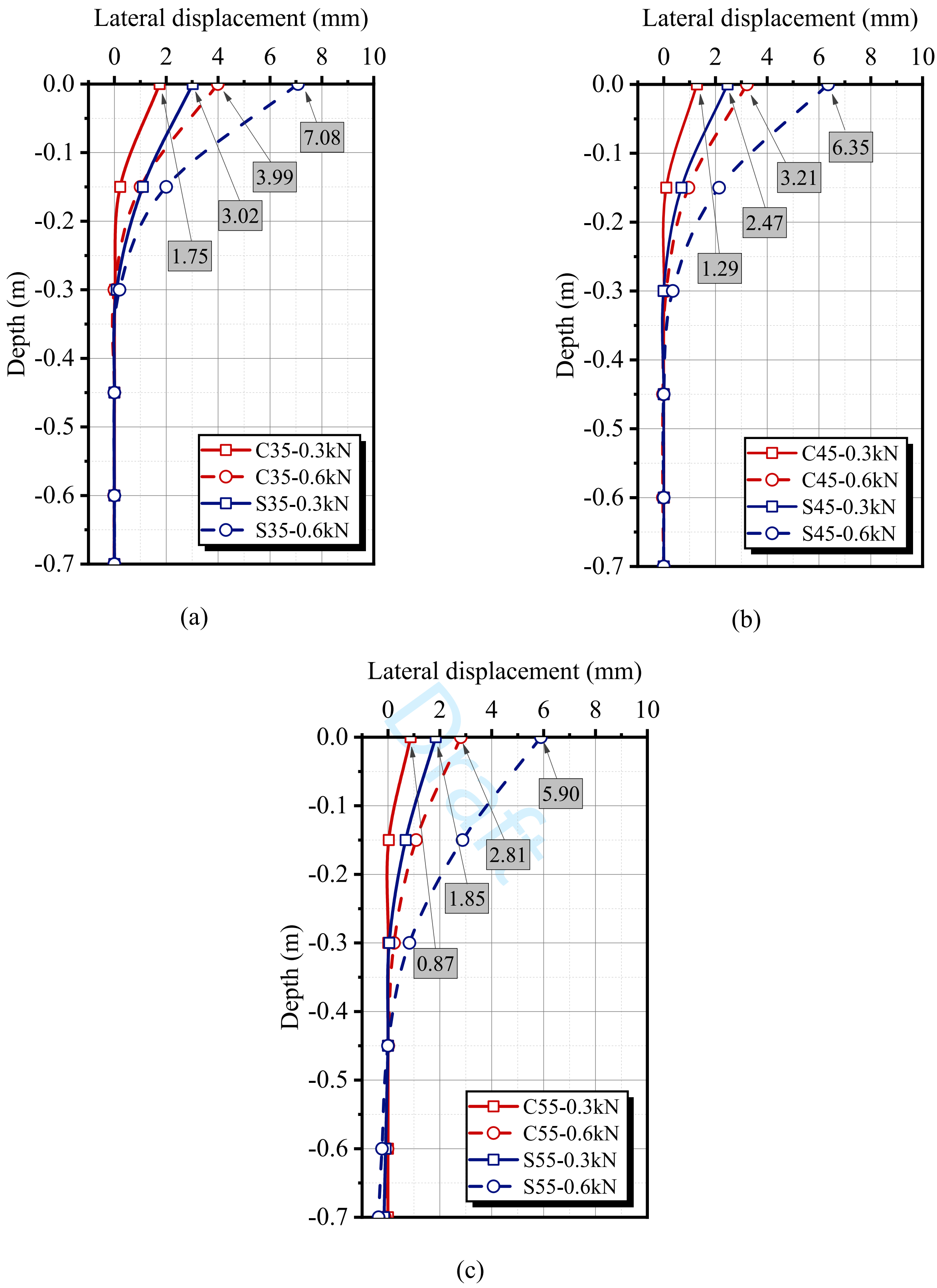

Figure 5. The lateral displacements of piles along depth at different load levels: (a) D=35 mm; (b) D=45 mm; (c) D=55 mm.

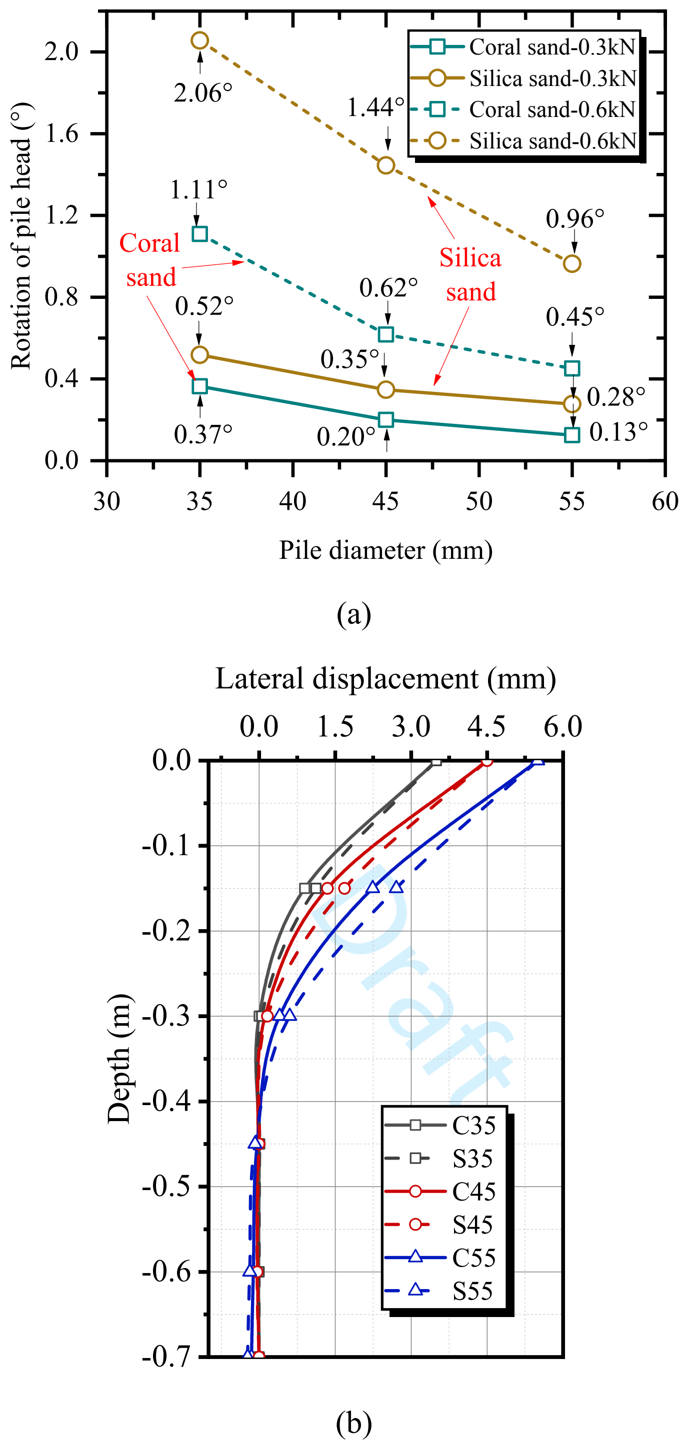

Figure 6. (a) Rotation of pile head at different loading levels; (b) Lateral displacements along pile depth when the lateral displacements at ground level reach 10%D.

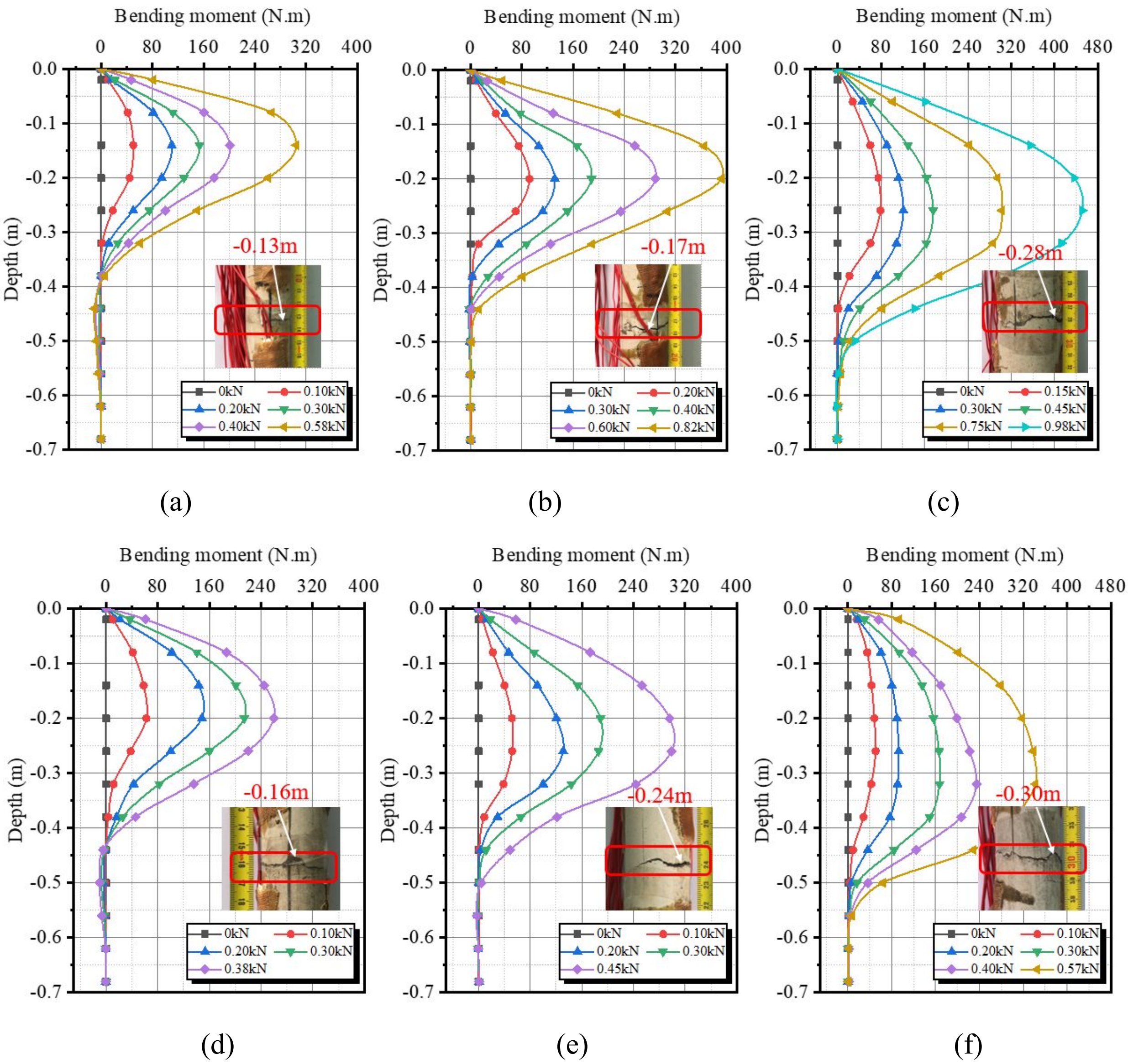

Figure 7. Distribution of bending moments of piles with different diameters; (a) C35; (b) C45; (c) C55; (d) S35; (e) S45; (f) S55.

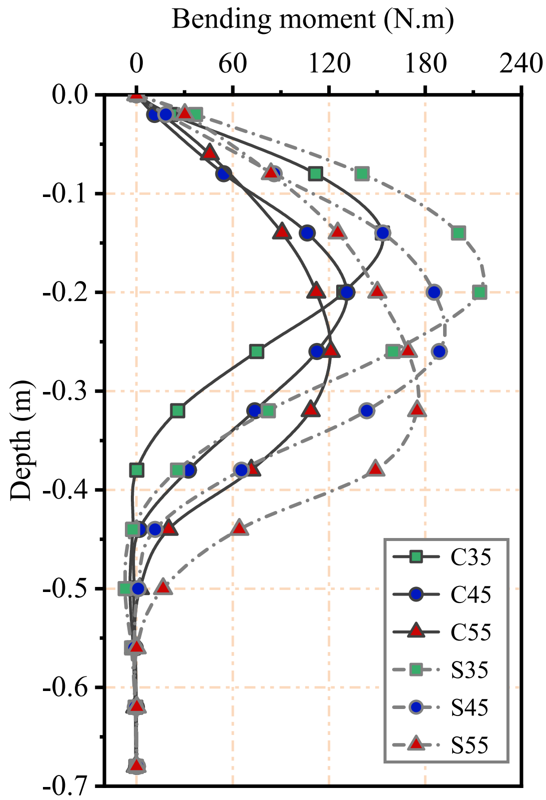

Figure 8. The comparison of bending moment at loading level of 0.3 kN.

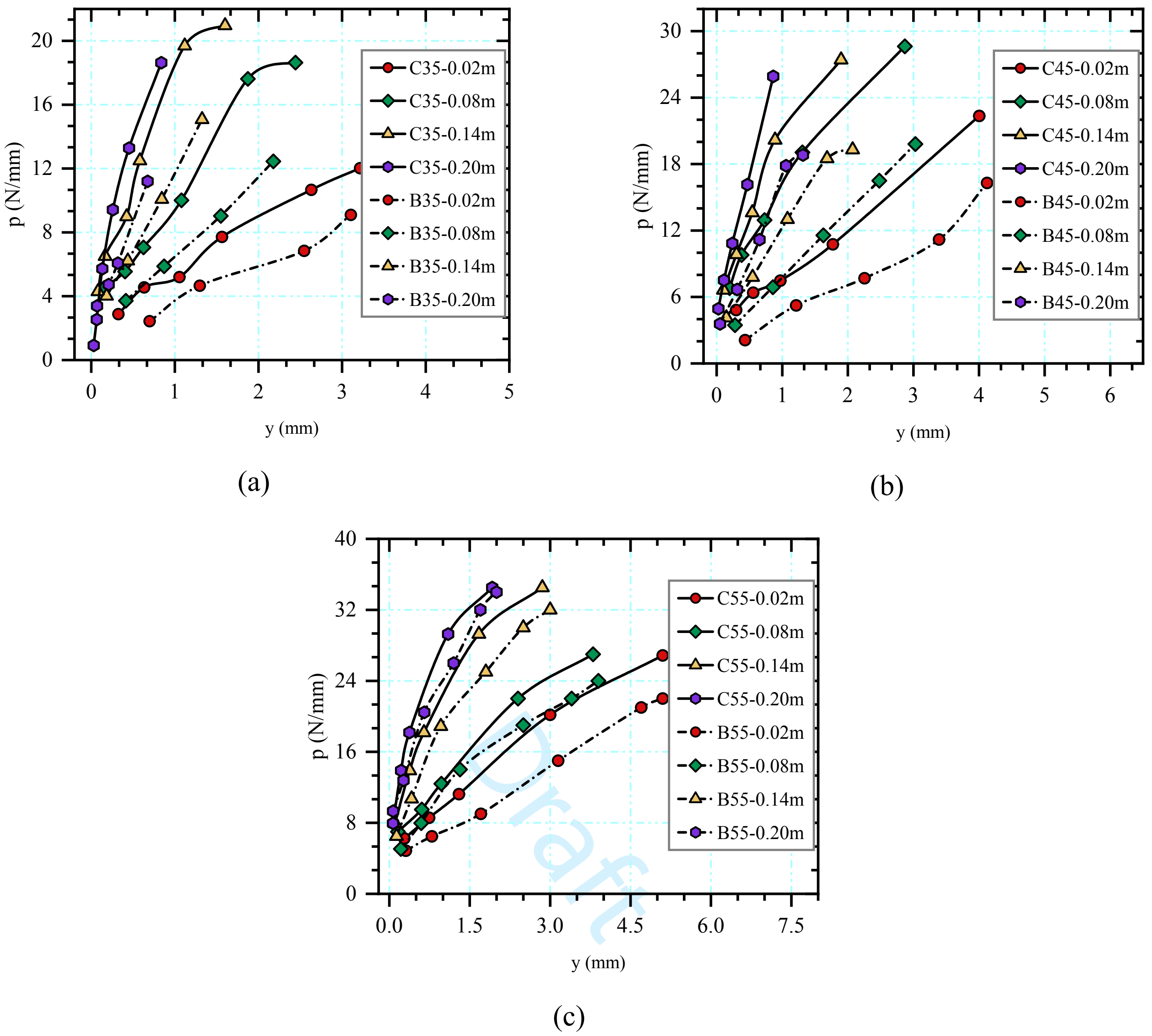

Figure 9. *P-y* curves at serval depths along the pile length: (a) *D*=35 mm; (b) *D*=45 mm; (c) *D*=55 mm.

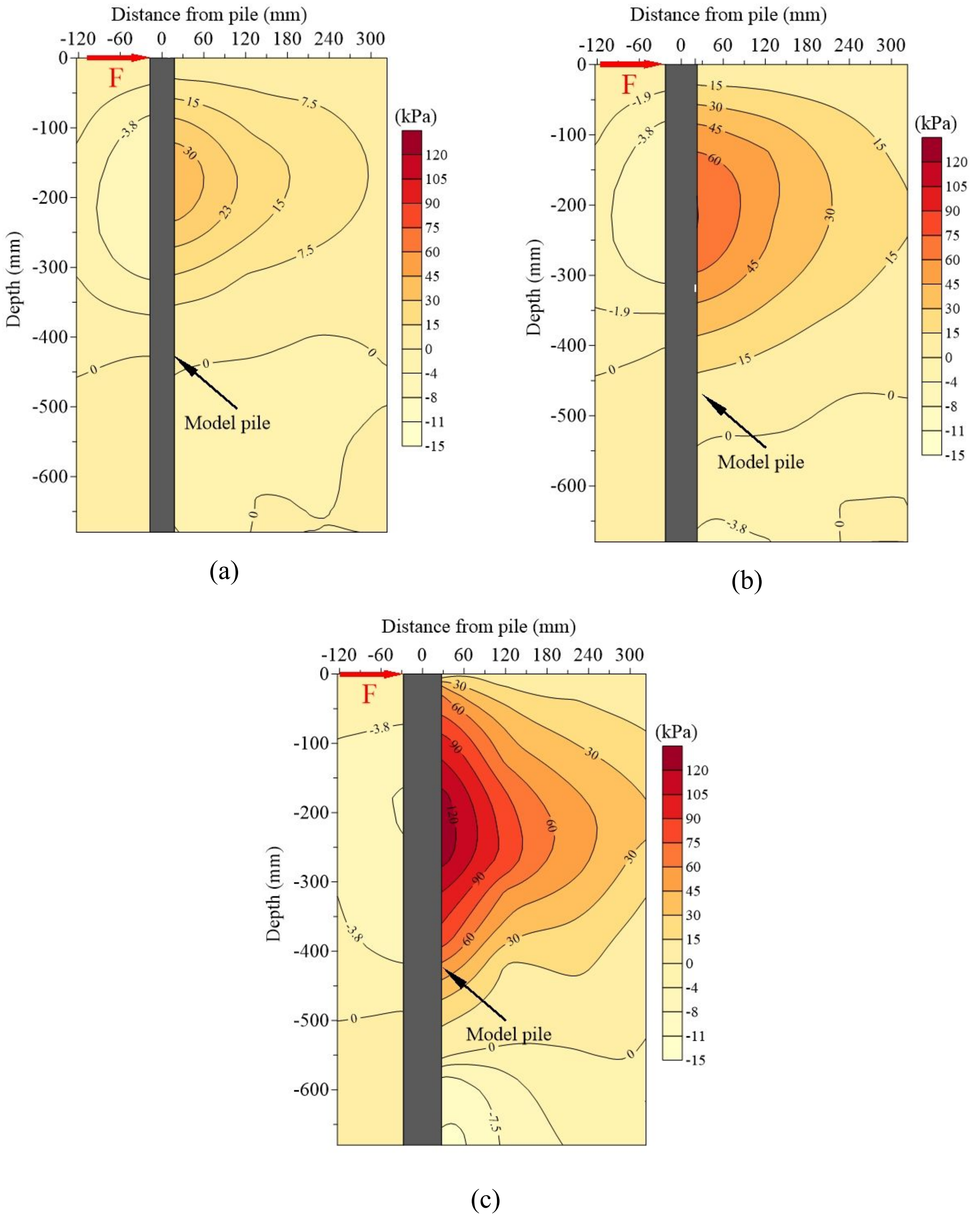

Figure 10. The changes in soil horizontal pressures of coral sand foundation: (a) C35; (b) C45; (c) C55.

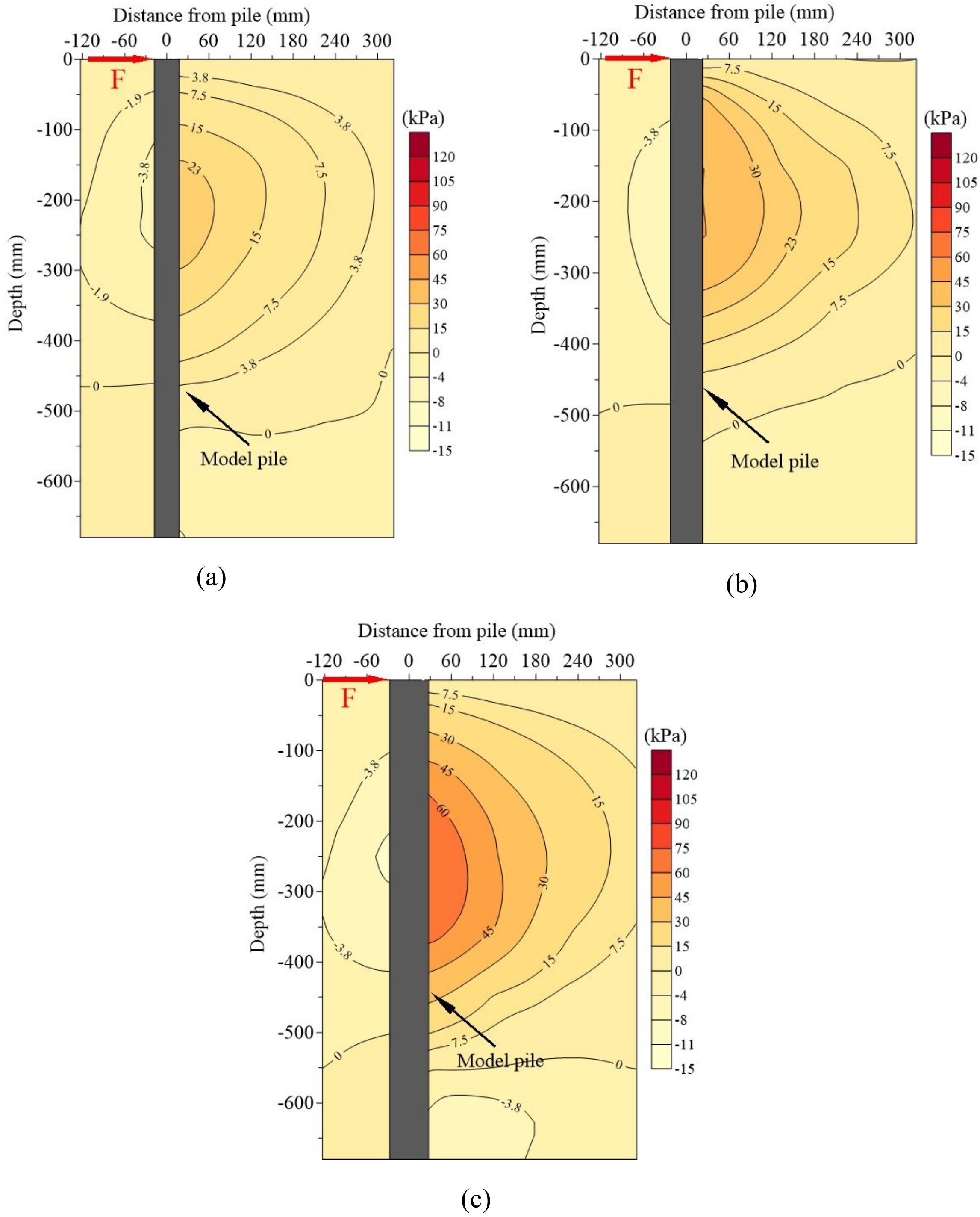

Figure 11. The changes in soil horizontal pressures of silica sand foundation: (a) S35; (b) S45; (c) S55.

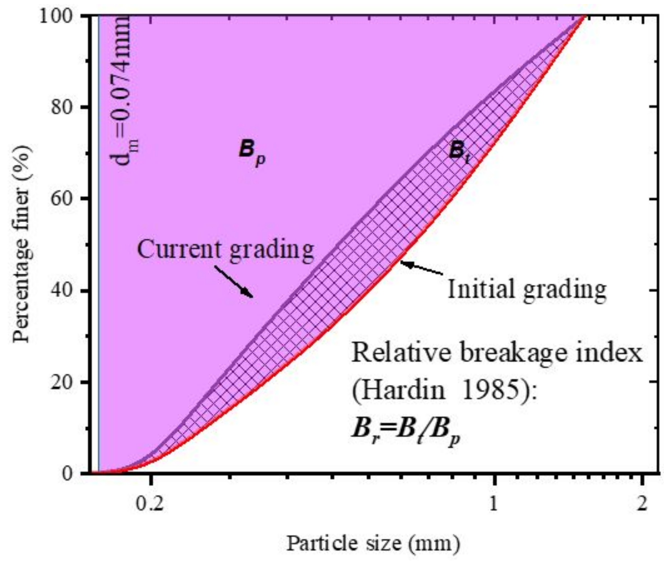

Figure 12. Definition of relative breakage index.

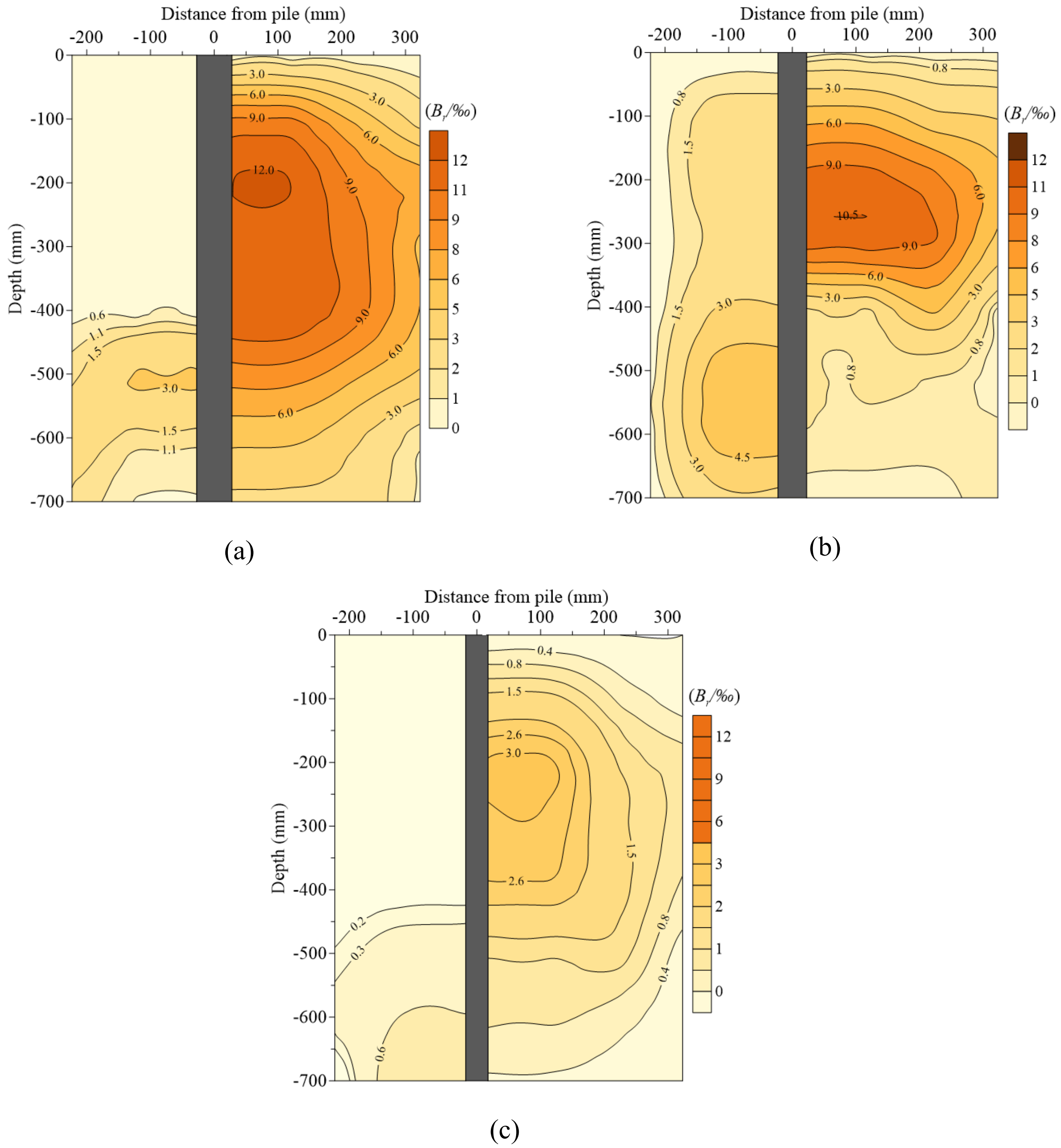

Figure 13. The distribution and level of particle breakage around the laterally loaded piles in coral sand: (a) C55; (b) C45; (c) C35.